A thin wire ion trap to study ion–atom collisions built within a Fabry–Perot cavity

Tridib Ray · S. Jyothi · N. Bhargava Ram · S. A. Rangwala

Abstract We report on the implementation of a thin wire Paul trap with tungsten wire electrodes for trapping ions. The ion trap geometry, though compact, allows large optical access enabling a moderate finesse Fabry–Perot cavity to be built along the ion trap axis. The design allows a vapor-loaded magneto-optical trap of alkali atoms to be overlapped with trapped atomic or molecular ions. The construction and design of the trap are discussed, and its operating parameters are determined, both experimentally and numerically, for Rb^+. The macromotion frequencies of the ion trap for $^{85}Rb^+$ are determined to be $f_r = 43$ kHz for the radial and $f_z = 54$ kHz for the axial frequencies, for the experimentally determined optimal operating parameters. The destructive off axis ion extraction and detection by ion counting is demonstrated. Finally, evidence for the stabilization and cooling of trapped ions, due to ion–atom interactions, is presented by studying the ion-atom mixture as a function of interaction time. The utility and flexibility of the whole apparatus, for a variety of atomic physics experiments, are discussed in conclusion.

1 Introduction

Trapping and cooling of ions have enabled the study of many interesting problems, ranging from sensitive tests of QED, fundamental interactions, quantum simulators for magnetism, quantum computation, etc. [1–4]. On the other hand, magneto-optically trapped (MOT) cold atoms and Bose–Einstein condensates have enabled the study of

quantum nature of interactions at very low temperatures [5, 6]. Hybrid traps simultaneously trapping ions and cold atoms open the possibility of relatively strong interactions in dilute gas systems [7]. Applications ranging from collision studies and few particle processes to ultracold chemistry [8–16] have been experimentally demonstrated with the mixed ion–atom experiments.

These hybrid traps utilize a linear Paul trap [17–19] as this gives the large amount of optical access required. Here, we develop a modified quadrupolar Paul trap using thin tungsten wire electrodes with large optical access such that it is geometrically consistent with the requirements of the experiment. The design of this ion trap is inspired by a configurationally similar wire trap for neutral cold polar molecules [20]. Further, the precise design of the trap is motivated by the need for overlapping the trapped ion–atom mixture with the mode volume of a moderate finesse optical cavity, so that entirely new methods of manipulating and detecting the mixtures can be developed. In this paper, we present the ion trap, its numerical and experimental characterization, and demonstrate that this is a robust system for experiments with trapped ion–atom mixtures.

2 Ion trap

2.1 Overview of the trap

The ion trap described here is at the heart of the compact setup along with a magneto-optical trap (MOT) and a Fabry–Perot cavity housed in a Kimball Physics™ vacuum chamber with sixteen CF16 and two CF100 ports. The instrument is designed to trap alkali and alkaline earth ions as well as their molecular ions. The ion trap is constructed at the geometric center of the chamber such that it is well

T. Ray · S. Jyothi · N. B. Ram · S. A. Rangwala (✉)
Raman Research Institute, Sadashivanagar,
Bangalore 560080, India
e-mail: sarangwala@rri.res.in

overlapped with the MOT and the cavity axis. The presence of the wire trap does not prevent the formation of a typical, vapor loaded MOT at the center of the chamber. The creation of a MOT within this wire trap structure and the strong coupling between the MOT atoms and the cavity have been demonstrated and characterized in at length Ray et al. [21]. However, in that article, the presence of the wire trap had not been explicitly discussed, as the emphasis was on the collective strong coupling of the laser cooled atoms and the Fabry–Perot cavity. Here, we remark that the diffraction effects of these wires does not hinder the formation of the MOT. We also ensure, by design, that the center of the MOT is not occulted by the shadow of the wires. This results in the creation of a well-behaved and characterizable MOT [21]. Here, we focus on the performance of the ion trap for mixed ion–atom species experiments keeping in mind the other aspects of the apparatus.

The wire trap consists of 4 square-shaped loops of tungsten wires of diameter 80 μm, separated by 1.5, 3 and 1.5 mm, respectively, and held taut by winding over a scaffolding provided by four stainless steel (SS316) rods in quadrupolar geometry (Fig. 1a). The wires are electrically isolated by ceramic spacers. The inner two wires are supplied with a time varying radio-frequency (rf) voltage, and the outer wires are held at a constant DC voltage with respect to the experimental ground. The rods around which the wires are wound can themselves be biased in order to
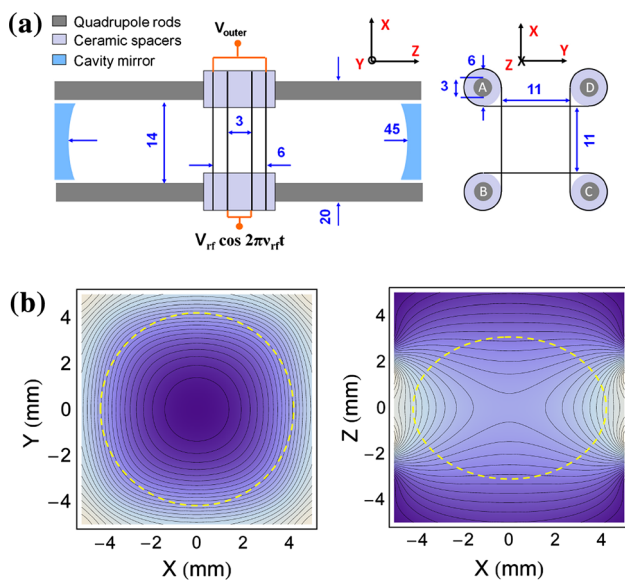

Fig. 1 a Side and axial view of the ion trap containing 4 square-shaped tungsten wires wound over four quadrupole rods *A, B, C,* and *D*. The outer pair of wires are biased with constant voltage V_{outer}, and the inner pair of wires are biased with a time varying radio-frequency voltage V_{rf} at frequency ν_{rf}. All dimensions are in mm. **b** Potential profile in XY and XZ planes passing through the trap center. The spatial extent of the stable trapping region is contained within the *dashed line*, the criterion for which is discussed in Sect. 2.8

influence the position and trajectory of ions. These are normally kept at the ground potential while the trap is in operation and can be rapidly switched to appropriate DC voltage to extract the ions onto a channel electron multiplier (CEM). Care is taken to screen the voltage on the piezo stack, attached to one of the mirrors of the cavity, from the trapping volume. The appropriate voltages and the frequency for trapping are determined by simulations apriori and then validated by experiments, as elaborated in sections below. The design and trap characteristics are simulated in SIMION™ and Mathematica™. Potentials were generated using SIMION™ for the inner and outer pair of wires. The entire potential environment of the vacuum chamber including the CEM is simulated, so that the boundary conditions for the trap operations were realistic. The potential array is then imported into a Mathematica script, where the ion trajectories for single ions as well as multiple ions are solved for, with the desired accuracy.

2.2 Creation of cold Rb atoms and daughter ions

The magneto-optical trap has been a common technique for creating cold atomic ensemble. In our setup, a MOT of ^{85}Rb atoms is created at the center of the chamber (which is also the center of the ion trap)—using three mutually orthogonal pairs of counter propagating laser beams intersecting at the center. The gradient magnetic field for the MOT is produced by coils situated outside the vacuum system, which can be aligned to match the centers of the various traps in the experiment. The presence of the multiple non-magnetic electrodes and structures in the close vicinity of the MOT capture volume does not have significant adverse effects on the laser cooling process [21].

The ion trap is loaded with ions created by 2-photon ionization (TPI) [22] of ^{85}Rb atoms in the MOT. The ionization potential (IP) of Rb atom is 4.18 eV [24]. The two photons for ionization here come from the MOT laser (1.59 eV) and a blue laser (Toptica Ibeam smart $\lambda = 473$ nm / 2.63 eV). Since the MOT cooling laser is just slightly red detuned with respect to the atomic transition, $5S_{1/2}(F = 3) \leftrightarrow 5P_{3/2}(F' = 4)$, the process is $1 + 1$ resonant TPI. The sum of the energy carried by the red and blue photons is ~ 4.22 eV, slightly higher than the IP of the Rb atom. The ions created have kinetic energy comparable with MOT atoms upon ionization. Since these ions are created from the MOT which is aligned to be at the geometric center of the ion trap, loading of the ion trap is very efficient. The daughter ions can easily be accumulated in the ion trap. However, with the passage of time post ionization, the ions are subjected to various heating mechanisms and therefore require a cooling mechanism to continue remaining trapped. When held together with the parent cold atoms, the ions are sympathetically cooled [16,

23]. This leads to stabilization in trapped ion number and long lifetime of the $^{85}Rb^+$ ions in the present setup, which is demonstrated below.

2.3 Trapping the ions

While the atoms are ionized, the trap should be operational to contain the ions. The trapping potential is generated by applying a rf voltage (V_{rf}) on the inner pair of wires. This produces a time varying saddle between the radial and the axial directions, as shown in Fig. 1b, providing an effective trapping potential for the ions. A DC voltage on the outer pair of wires can be applied to modify the trap depth in the radial and axial directions. Also, an asymmetric DC voltage combination can be used to translate the ion trap center along the axis in order to have maximum overlap with the MOT atoms. The time varying rf signal is produced in a function generator (Agilent: 33512B) and amplified using a wide band rf amplifier (Krohn-Hite: 7602M). The typical range of the parameters used for trapping ions is 400 kHz $\leq v_{rf} \leq$ 600 kHz and 70 V $\leq V_{rf} \leq$ 120 V. The static voltage on the outer pair of wires is in the range -15 V $\leq V_{outer} \leq$ 10 V.

The region of stability for a single ion is determined by simulating the trajectories of a Rb^+ ion with zero initial energy, over 200 rf cycles for a combination of V_{rf} and V_{outer} values and checking whether it is confined within the volume of the trap. Figure 2a, b shows the stability characteristics of trapped $^{85}Rb^+$ ions obtained at 500 kHz rf frequency. The approximate spatial extent of the potential for stable $^{85}Rb^+$ ion trapping is contained within the dashed line in Fig. 1b.

2.4 Detection of ions

The lack of accessible optical transition in Rb^+ ion due to its closed shell structure makes fluorescence detection impractical. In the present experimental setup, a CEM (Dr. Sjuts KBL10RS) is used to detect the ions. Since the cavity and the ion trap share the same axis, axial extraction of the ions is not possible. In this experiment, the CEM is placed perpendicular to the cavity axis (along y-axis) at a distance of 44.5 mm from the trap center as shown in Fig. 3a. The CEM is housed in a metallic box, and a mesh is used in front of the cone to shield the high voltage from altering the ion trap potential. The CEM cone voltage is -2.4 kV, and the mesh is biased at -120 V for efficient extraction. The trapped ions are extracted toward the CEM by switching the left side pair of the quadrupole rods, A and B, to $+400$ V and keeping the right side pair of rods, C and D, at 0 V (Fig. 3a). The switching of the extraction voltages on the quadrupole rods is done using a Behlke^{TM} (HTS-31) high voltage switch. A symmetric potential profile along
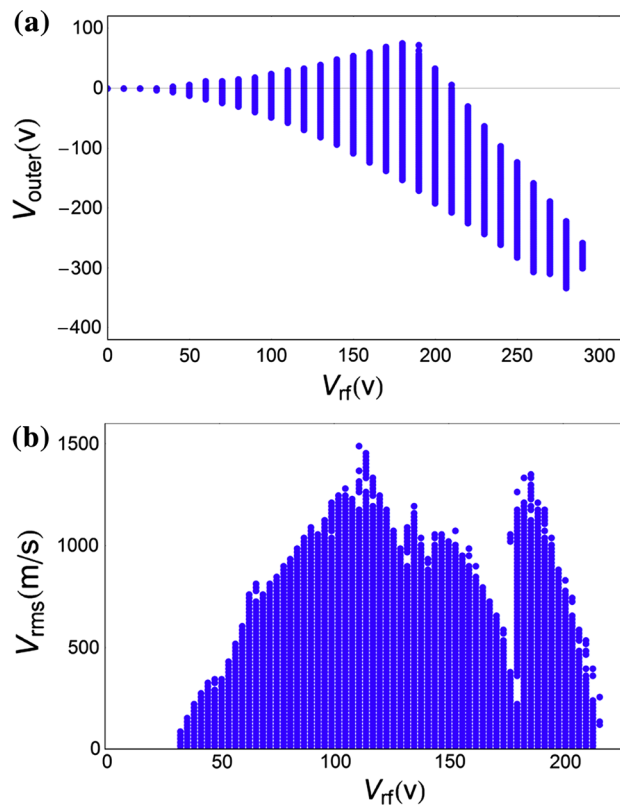

Fig. 2 **a** The region of stability for a single Rb^+ ion in the trap for a combination of V_{outer} and V_{rf} at rf frequency 500 kHz. **b** Stability plots showing maximum trappable rms velocities of a single Rb^+ ion as function of V_{rf} for $V_{outer} = -5$ V and $v_{rf} = 500$ kHz. Both the figures are obtained by solving single particle equation of motion in the SIMION generated trapping potential as described in Sect. 2.1

the y-axis to guide the ions to the CEM with minimum loss is maintained. The time of flight of the Rb^+ ions is measured to be around 5 μs (Fig. 3b). The precise position and width of the arrival time sequence of the ions depend sensitively on the timing of the extraction pulse with respect to the rf phase [19]. For the present experiment, we have ensured that the ion extraction is maximally efficient for detection. The precise dependence of the ion signal on the phase at which the ions are extracted will be reported elsewhere.

2.5 Counting the ions

To determine the number of ions extracted onto the CEM precisely, two schemes are employed. These are the *pulse counting* and the *integration mode*. In the pulse counting scheme, the arrival of the ions on the CEM creates a corresponding train of current pulses. These are converted into a voltage signal and measured as 8ns wide negative irregular pulses with amplitudes ranging from a few to several ten milli Volt per pulse. The pulse train is recorded in a digital storage oscilloscope (DSO), and then, the
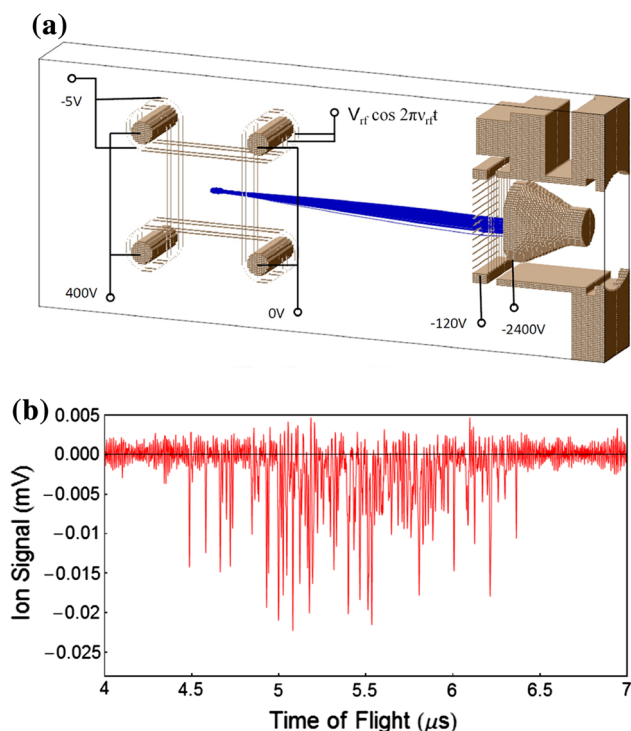
(a)

(b)

Fig. 3 a The voltage configuration on the electrodes for ion extraction onto CEM is shown. The *blue solid lines* show the ion trajectories in the extraction field as simulated in SIMION. **b** illustrates a high density ion signal from the CEM in the pulse counting mode. In parts of the signal, ion pileup can be seen

number of pulses is counted using an appropriately set discriminator level [22], of approximately 4 mV in the present experiment. Negative peaks with amplitude greater than the discriminator level are counted while the smaller peaks are discarded as noise. Since the data are recorded and therefore always available, it allows for a variety of postprocessing. A drawback of this scheme is the inability to identify pileup of ions which occurs due to the arrival of more than one ion within the 8ns pulse width, limiting the reliable count rate to a few hundred ions per 10 μs. The advantage is that a robust algorithm for pulse counting allows data from several runs to be analyzed in a uniform manner.

In the integration mode, the CEM signal is fed into a low bandwidth amplifier with set amplification factor, and the output is recorded on a DSO. The area under the curve, measured in V μs unit, and a proportionality is established to the number of ions detected. A calibration between the pulse counting mode and the integration mode gives the constant of proportionality as 5.11 ± 0.23 ions per V μs. It should be noted that this constant of proportionality is dependent on the CEM bias voltage, the amplifier gain and cut-off frequency. This scheme potentially allows higher ion count rates.

2.6 Optimal trapping conditions for Rb^+

In this experiment, at a suitable rf frequency of operation (500 kHz), the optimal trapping of the Rb^+ ions relies on two parameters, V_{rf} and V_{outer}. Optimal trapping conditions should ensure long lifetime of the ions and is experimentally determined in two steps. In the first set of experiments, the number of trapped ions is counted as a function of V_{rf}. The experiments are repeated at different values of V_{outer} as shown in Fig. 4a. The shift in the trapping region with V_{outer} can be explained from the stability diagram (Fig. 2a). More negative values of V_{outer} increase the threshold and reduce the range of V_{rf} for stable trap operation. The study allows us to choose $V_{rf} = -5$ V as a good operating point, as at this value the trap depth is close to maximum, with a lower threshold for ion trapping and wide range of experimentally accessible V_{rf} values. The high frequency cutoff of V_{rf} in this experiment comes from the imperfection of the rf arising due to the gain-bandwidth saturation of the amplifier. With the chosen value of V_{outer}, the number of ions in the trap, when held together with the
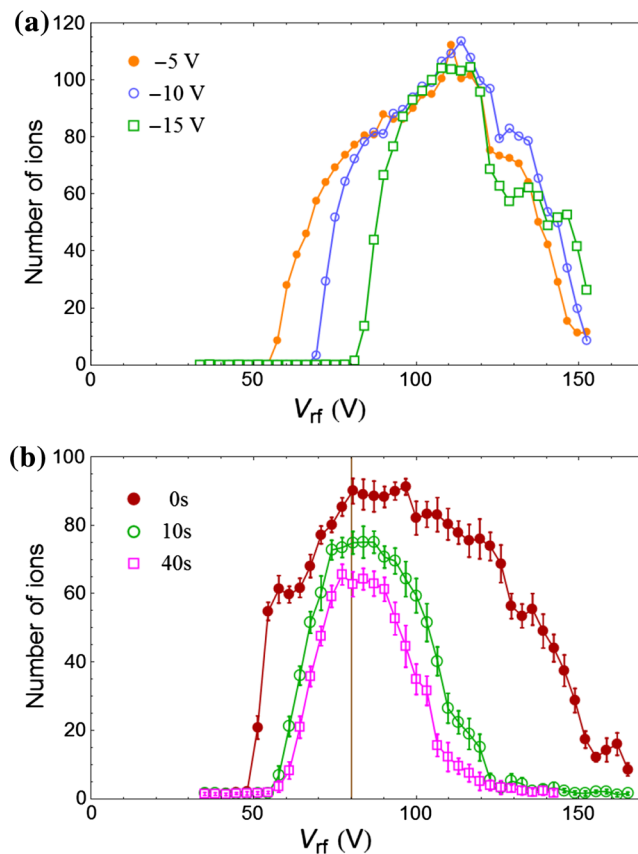
(a)

(b)

Fig. 4 Variation in number of trapped ions detected as a function of V_{rf} at 500 kHz for **a** different values of V_{outer} and **b** different trap hold time at $V_{outer} = -5$ V. All the above measurements were done with the trapped ions overlapped with the cold Rb atoms in the MOT. The standard deviation error bars are shown in **b**

cold atoms, is measured as a function of V_{rf}. Figure 4b shows the results for different holdtimes. For longer holdtime, the stable V_{rf} regime shinks, allowing us to find out ~ 80 V as the most stable V_{rf} of operation for the given trap parameters.

2.7 The secular motion and motional resonances

The dynamical trapping of ions in a radiofrequency trap leads to motion of the ion that can be decomposed into micromotion and macromotion. The former is induced by the driving rf field and has the same frequency as the driving field. The latter is a slower orbital motion caused by the effective trapping potential. Experimental determination of the macromotion frequencies is done by first trapping ions at the good operating point established above and then applying a weak rf perturbation, whose frequency is scanning, to the V_{rf}. The perturbation, when in resonance with the macromotion frequencies, results in rapid heating of the ions leading to their ejection from the trap. Figure 5 shows the macromotion resonance spectrum of the Rb^+ ions obtained at $V_{rf} = 80$ V, $V_{outer} = -5$ V and $\nu_{rf} = 500$ kHz. Several resonances are identified as the fundamental, harmonic and sub-harmonic frequencies corresponding to the oscillation of the Rb^+ ions. From the excitation spectrum in Fig. 5, we find the resonance frequencies f_z and f_r to be 54 and 43 kHz, respectively.

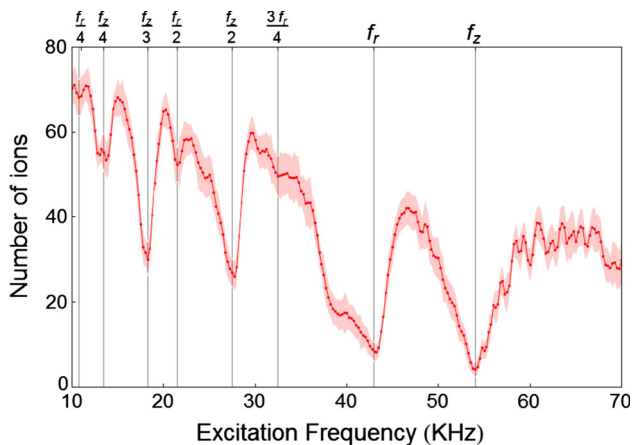The macromotion resonance frequencies above are independently determined from simulations. Here, the equation of motion of a single ion is solved for 5,000 cycles, in the potential obtained using SIMION™, for the optimized trap parameters. The macro motion frequencies in radial and axial directions are found from the power spectrum of the particle trajectories in the corresponding directions. The measured frequencies agree to within a few percent with the macromotion frequencies obtained from the ion trap simulations.

2.8 Estimation of trap extent and trap depth

Finally, we determine the secular trap depth at the above optimized operating parameters by determining the maximum spatial displacement that an ion can be subjected to, with zero velocity, and be still be trapped. It is found from simulations that this distance along the x and y axes is 4.2 mm and the displacement is 3.0 mm along the z direction as shown in Fig. 6. This is consistent with the potentials illustrated in Fig. 1b. Substituting these values for maximal displacement into the harmonic oscillator potential energy expression,

$$U_{x,z} = \frac{1}{2} m (2\pi f_{x,z} \Delta_{x,z})^2,$$

where m is the mass of the Rb^+ ion, $U_{x,z}$ is the maximum secular potential energy, $f_{x,z}$ is the experimental secular frequencies and $\Delta_{x,z}$ is the maximum displacement in the x and z directions, respectively, we obtain the secular trap depth. On substitution, the secular trap depth is lower in the z direction and has a value of $U_z = 0.46$ eV, which can be regarded as a reliable upper bound on the trap depth.
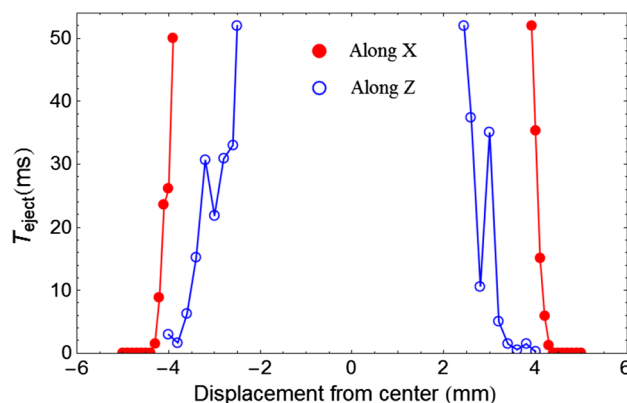

Fig. 5 Motional resonance spectrum of trapped Rb^+ ions measured at $V_{rf} = 80$ V, $V_{outer} = -5$ V and $\nu_{rf} = 500$ kHz. The trapped ions are held for 10 ms during which a low power rf voltage is mixed in with the V_{rf} and applied to the inner wires. The figure illustrates the variation in the ion counts as a function of the excitation frequency, where each point represents the average of 20 measurements, comprising a full cycle of ion creation, trapping, excitation and ion detection. The *shaded area* represents the standard deviation error. Frequencies where the ion motion is resonant lead to loss of the ions from the trap and consequently low ion yield detected on the CEM

Fig. 6 The time spent (T_{eject}) by the ion in the trap before it ejects when initial position is displaced along x or z direction is shown. This illustrates the maximum extent of displacement of a trapped ion along the x and z axis. The extreme values represent the outermost turning point for an ion with zero velocity and therefore the overflow point of the secular trap. The asymmetry along z axis is due to the presence of unbiased electrodes in the setup causing a slight asymmetry in the potential. Therefore, in the z direction, we take the lower of the two values and define the trap extent as 3.0 mm from the origin
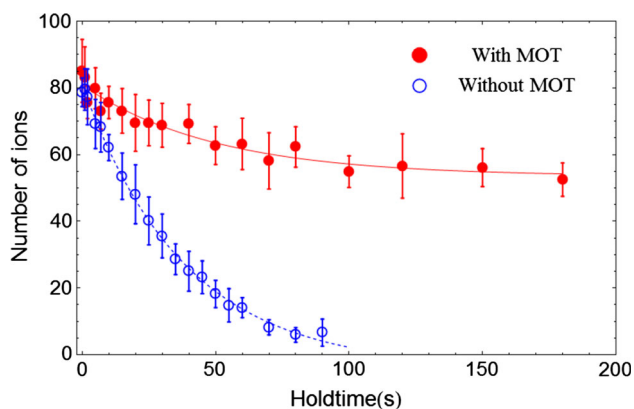
Fig. 7 Plot showing ion yield as a function of hold time in absence and presence of the MOT. Presence of the MOT leads to longer ion lifetimes attributed to sympathetic cooling. *Solid lines* are exponential fits without or with an offset for the respective experiments. The standard deviation *error bars* are shown

3 Ion–atom interactions: stabilization of Rb$^+$ ions

The lifetime of the ions in an imperfect trap is finite. The loss of ions from the trap due to heating is caused by mainly two factors. Deviation of the trap potential from the ideal quadrupole form and collision induced phase change. However, when the ionic ensemble is held together with the localized parent cold atoms, they are cooled by elastic and resonant charge exchange collisions. This leads to stabilization of the number of ions in the trap as has been shown in earlier work [16, 23]. The present experimental system, as shown in Fig. 7, shows a significant improvement over our earlier work [16] in the lifetime of the trapped ions. In the absence of the cold atoms, the ion lifetime in the trap has improved significantly, and a much larger fraction of ions is stabilized when held together with the cold atoms, indicating that the combined ion–atom trap presented here is robust. This establishes the instruments capability for studying ion–atom mixtures within a Fabry–Perot cavity.

4 Discussion, conclusion and science directions

The above experiment characterizes a novel thin wire ion trap design and discusses its implementation. This comprises a crucial part of a versatile an atomic physics experiment, which brings together ion and atom cooling and trapping, cold molecules and integrates these three systems such that they can be simultaneously in the cavity mode volume. The configuration of ion trap described here is conceptually adapted from the spherical Paul trap design. This design is generic in the sense that a change in the geometry would result in the change in the operating voltages and frequencies for a particular ion, but could be

expected to trap ions with comparable results. The reason for our specific wire trap dimensions is that the present wire trap can also be used to trap neutral dipolar cold molecules [20], and our dimensions are adapted for this. Here, the ion trap is characterized, optimized and operated, allowing the simultaneous spatial trapping of cold atoms and ions and demonstrating their interactions. These experiments can be done in steady state, as the ion and atom numbers can be held constant by loading and then time evolution of the mixed system. The open geometry of the trap enables large optical access and allows the trap to be placed within a Fabry–Perot resonator, allowing not just the cold atoms [21] but the ion–atom mixture to be probed by the Fabry–Perot cavity around the trap.

In addition, our thin wire trap structure can also be used to impose a strong, constant electric field for atom or molecule alignment studies, using the cavity as detector. Of course, in this case, the ions cannot be trapped simultaneously, due to the presence of strong constant electric fields. This flexibility, along with the possibility of trapping neutral molecules, sets the present thin wire ion trap apart from the segmented electrode linear Paul trap, which is also consistent with an axial cavity. Clearly, this combination, which allows the mixing of cold atoms, trapped and cooled ions and good quality cavity, is formidable, and a variety of interesting measurement possibilities are enabled. Further, the setup allows more than one species of ion and/or atoms to be loaded simultaneously, and the interactions among the different species can be probed.

References

1. D. Leibfried, R. Blatt, C. Monroe, D. Wineland, Rev. Mod. Phys. **75**, 281 (2003)
2. K. Blaum, Y. Novikov, G. Werth, Contemp. Phys. **51**, 149 (2010)
3. J. Ye, H.J. Kimble, Hidetoshi. Katori, Science **320**, 1734 (2008)
4. A.J. Leggett, Rev. Mod. Phys. **73**, 307 (2001)
5. W. Ketterle, D.S. Durfee, D.M. Stamper-Kurn, *Proceedings of the International School of Physics "Enrico Fermi"*. Course CXL, (1999), pp. 67–176
6. W. Ketterle, M.W. Zwierlein, La Rivista del Nuovo Cimento **5**(6), 247–422 (2008)
7. R. Cote, V. Kharchenko, M.D. Lukin, Phys. Rev. Lett. **89**, 0930001 (2002)
8. W.W. Smith, O.P. Makarov, J. Lin, J. Mod. Opt. **52**, 2253 (2005)
9. S. Willitsch, M.T. Bell, A.D. Gingell, S.R. Procter, T.P. Softley, Phys. Rev. Lett. **100**, 043203 (2008)
10. A.T. Grier, M. Cetina, F. Orucevic, V. Vuletic, Phys. Rev. Lett **102**, 223201 (2009)

11. W.G. Rellergert, S.T. Sullivan, S. Kotochigova, A. Petrov, K. Chen, S.J. Schowalter, E.R. Hudson, Phys. Rev. Lett. **107**, 243201 (2011)
12. S. Lee, K. Ravi, S. A. Rangwala, Phys. Rev. A **87**, 052701 (2013)
13. F.H.J. Hall, M. Aymar, N. Bouloufa-Maafa, O. Duilieu, S. Willitsch, Phys. Rev. Lett. **107**, 243202 (2011)
14. S. Schmid, A. Harter, A. Frisch, S. Hoinka, J.Hecker Denschlag, Rev. Sci. Instrum. **83**, 053108 (2012)
15. M.T. Bell, T. P. Softley, Mol. Phys. **107**, 99 (2009)
16. K. Ravi, S. Lee, A. Sharma, G. Werth, S.A. Rangwala, Nat. Commun. **3**, 1126 (2012)
17. W. Paul, H. Steinwedel, Z. Naturforsch A **8**, 448 (1953)
18. J.D. Prestage, G.J. Dick, L. Malecki, J. Appl. Phys. **66**, 1013 (1989)
19. F.G. Major, V.N. Gheorghe, G. Werth, *Charged Particle Traps*. (Springer, Heidelberg, 2005)
20. J. Kleinert, C. Haimberger, P.J. Zabawa, N.P. Bigelow, Phys. Rev. Lett. **99**, 143002 (2007)
21. T. Ray, A. Sharma, S. Jyothi, S.A. Rangwala, Phys. Rev. A **87**, 033832 (2013)
22. K. Ravi, S. Lee, A. Sharma, G. Werth, S.A. Rangwala, Appl. Phys. B **107**, 971 (2012)
23. I. Sivarajah, D.S. Goodman, J.E. Wells, F.A. Narducci, W.W. Smith, Phys. Rev. A **86**, 063419 (2012)
24. J.E. Sansonetti, W.C. Martin, J. Phys. Chem. Ref. Data **34**, 1559–2259 (2005)